Rakenteiden Mekaniikka (Journal of Structural Mechanics)
Vol. 56, No. 1, 2023, pp. 24–40
https://rakenteidenmekaniikka.journal.fi/index
https://doi.org/10.23998/rm.120756

VERTAISARVIOITU
KOLLEGIALT GRANSKAD
PEER-REVIEWED
www.tsv.fi/tunnus

Durability of sandwich structures with a maximized natural raw material basis: comparison of expanded polystyrene, cellulose foam and polylactic acid subjected to UV-rain aging

P. Hakala[1], O. Orell, E. Sarlin, E. Pääkkönen, L. Jutila and M. Kanerva

Summary In this study, alternative core materials to commercial cork were searched for. Additionally, aging of new core materials was studied. Bio-based materials in sandwich structures can be useful for sports equipment, transportation, and furniture with much less impact on the environment in comparison with their synthetic counterparts. In this paper, sandwich panels made of fiber-reinforced polymer (FRP) skins and various sustainable core materials with a core thickness of 6 mm were studied. The core materials were: cork, expanded polystyrene (EPS), cellulose foam, and 3D-printed polylactic acid (PLA) honeycomb lattice. FRP composites made of flax fibre reinforcement and bio-based epoxy resin (30% bio-content) were used to manufacture the skins to compete the glass fibre reinforced rival composite. The experimental analysis of the panel performance focused on the out-of-plane behavior and aging due to conditioning in an ultraviolet (UV) irradiation-rain cabinet. The results showed that under mechanical and environmental loading, the sandwich composite with cellulose foam had comparable or even better mechanical performance under shearing load, including UV-rain effects, than structures with EPS cores. Failure localization was studied using digital image correlation (DIC). The 3D-printed PLA honeycomb sandwich structures had a high absolute flatwise tensile strength and shear strength but also greatest degradation by the UV-rain aging.

Keywords: bio composite, composite sandwich structure, thermoset resin, tensile strength, shear, failure

Received: 4 August 2022. Accepted: 30 January 2023. Published online: 2 May 2023.

Introduction

The use of sandwich structures with skin sheets made of fibre-reinforced polymer (FRP) and lightweight core material leads to the most weight-optimized components under bending loads. The sandwich concepts have been shown to be very effective in increasing overall strength and bending stiffness of structures [1]. The FRP skins can resist out-of-plane impacts and in-plane stresses under flexural deformations, while the core is required to resist shear stresses and prevent instability of thin skin sheets. The current partly biobased FRP sandwich structures in the traditional sandwich structure applications, such as water

[1]Corresponding author: pauli.hakala@tuni.fi

sport equipment or transportation, are gaining a lot of attention in the recent literature [1]. Nowadays, engineers aim, not only to improve strength-to-weight ratio in products, but also various environmental aspects.

To be more truly environmentally conscious, conventional materials and structures need to be re-evaluated to determine how they can become more sustainable through proper design procedures and reach smaller environmental impact during the manufacturing, installation, service and disposal phase of the product lifetime [2, 3, 4]. FRP composites made using synthetic fibres, such as glass or carbon fibres, are often applied to the skins of sandwich panels. The concept of using plant-based natural fibres, such as flax or hemp fibres, has also been increasingly explored for composites skins [5, 6]. Natural fibres have a lower strength than their synthetic counterparts but their density-normalized specific strength values are high. In addition, for some applications, the excellent damping properties of natural fibre FRPs are an advantage [7].

Sandwich panels might experience a multitude of types of failure modes, e.g., core shear, bonding failure, skin crushing or rupture and numerous instability modes [8]. Core materials that are commonly studied include synthetic foams and different honeycombs. Core also affects the damage tolerance often required for design [9]. Although flax has been studied previously for the use in sandwich structures, the combination of flax FRP with the latest bio-based core materials has yet to be studied in detail and analysed in terms of mechanical performance not to mention durability against environmental stress. In future, combinations of sandwich panel raw materials that are almost entirely composed of a natural stock (such as plant fibres or wood) can lead to a lesser impact on the environment compared to their synthetic rivals.

The aim of the study is to experiment, evaluate and compare the durability of bio-based and synthetic core materials in sandwich panels with FRP skin sheets. The test specimens are subjected to ultraviolet (UV) irradiation and moisture by using an UV-rain cabinet. The aging in the cores is measured in terms of changes in out-of-plane tension and shear performance. These panels are targeted to represent an alternative material system to conventional sport equipment and transportation vehicles where glass fibre and carbon fibre reinforced plastics are typical solutions for sandwich panels with foam cores based on the petrochemical industry. When compared to metallic cores, the manufacture and recycling of metals requires great amounts of energy due to the high enthalpy of fusion. On the other hand, poly(lactic acid) (PLA), cork, and cellulose can be industrially composted. Expanded polystyrene is well recyclable.

Materials and methods

Core splices

The material systems studied in this work are so-called sandwich panels. Sandwich panels are layered structures, where monolithic composite panels (i.e., skin sheets) confine a core splice in the middle so that a three-layer sandwich is formed. In this work, the main interest is the mechanical performance of material used for the core part.

The reference material system (REF-G), representative of rival application, is a sandwich panel with glass reinforced polyester skin sheets and cork core (see Table 1 for cores). This sandwich is a cost-efficient solution but rather heavy due to the relatively high density of the cork core splice and glass fibre reinforcement. Alternative core and skin materials were studied to compete the reference in terms of sustainability and light-weightiness. Here, sustainability refers to bio-based raw materials as well as the ability to recycle. Of

all the core materials (Table 1), cork represents entirely natural material with the least processing. The cellulose (CS) foam is natural material yet outcome of a laboratory-scale processing method [10]. EPS is a polystyrene foam but can be almost completely recycled. PLA represents a type of biopolymer that can be produced of biomass and composted in specialized processes.

The densities of the selected cores can be varied. Cork, being tree bark, can be harvested and certain batches can be found with different densities (here, the grade NL20 of 200 kg/m^3 was selected). Foam-formed cellulose structure was prepared in a lab scale. Bleached softwood kraft pulp fibres (Metsä Fibre Oy, mean fibre length 2.2 mm) were mixed with water, polyvinyl alcohol (PVA Poval 6-88, Kuraray, dosage 0.1 g/g fibre) and 3 w-% of chitosan. Pulp slurry was mixed 3000 rpm to the 32 % air content. Wet foam was poured into a 43 × 43 cm sheet mould with a mesh on the bottom. Cellulose foam was dried over night at 70 °C in an oven. The dry sheet was rewetted up to 50 % moisture content and pressed to the target thickness of 20 mm and dried between plates in the oven. The final dry sheets' properties were measured after conditioning (23°C, 50 % RH), and were: grammage 1320 g/m^2, thickness 20 mm and density 66 kg/m^3. The PLA core was 3D-printed honeycomb core. The PLA core was 3D-printed using PLA strand (type 1.24 g/cm^3, EasyFil PLA, Formfutura). Honeycomb is certain (common) three-dimensional geometry typical of high-performance sandwich cores. Honeycomb is characterized by its cell dimensions (Fig. 1). Different dimensions were studied—finally capping without an angle was used.

Table 1: The core material candidates used in this study. All the core splices had a splice thickness of 6 mm.

Core material	Grade	Manufacturer, notes	Density
Cork	Corecork NL20	Amorim Cork Composites	200 kg/m^3
EPS	Symbra	Bewi	30 kg/m^3
Cellulose	Foamed	Laboratory-developed [10]	66 kg/m^3
PLA	EasyFil PLA	3D-printed honeycomb	547 kg/m^3

Composite skin sheets

For the REF-G series, the sandwich panels were manufactured by using filament winding in order to the mould and directly bond composite skins to the core surface. Commercial glass fibre yarn (E6CR17-2400-386, Jushi) and an unsaturated polyester (UP) resin system (M300 TBR, Ashland Composite Polymers) were used.

Representing a more sustainable option compared to REF-G sandwiches, flax reinforced composite skins were prepared for the candidate sandwich panels. For the flax reinforced composite skins, commercial flax reinforcement (2/2 twill, 200 g/m^2, Composites Evolution (Biotex)) and partly bio-based (30% bio-content) epoxy resin (Super Sap One, Entropy Resins) with hardener (Super Sap ONF, Entropy Resins) were used with a mixing ratio of 100:43 by weight. The skin laminates were prepared under vacuum bag (vacuum pressure -0,6 bar) and post-cured for 24 h at 50 °C. The flax-epoxy skin laminates were prepared with three layers of flax (lay-up [90/45/90]).

The PLA matrix composite skins were prepared by hot pressing. 4 layers of flax was used and pre-pressed PLA layers in between. The stack was pressed by using a hot press

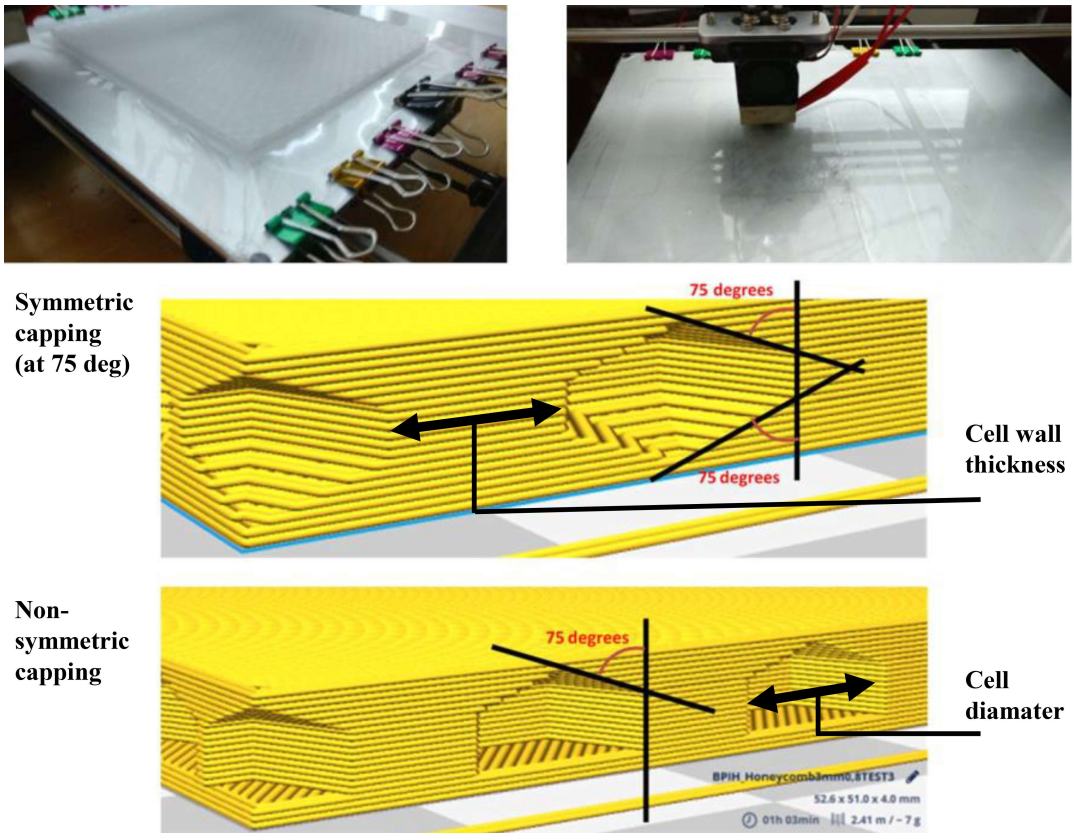

Figure 1: Characteristics of the PLA honeycomb core.

(MKH press, Tarkmet), using 2 bar of pressure, and at a temperature of 180 °C. The hold period was 10 minutes. Reinforcement lay-up was adjusted according to wetting by PLA and epoxy, and resulting thicknesses of skin laminates.

Core bonding

The core splices were bonded to the skin sheets by using three alternative methods. The raw materials and the different bonding methods formed the basis of test series. Test series of this study are shown in Table 2. The first method (Co) was direct co-lamination of the skin composite on top of core; the bonding process is faster when bonding and cure of the skin sheet occur at the same time. The rival (REF-G) and EF-EPS-Co series were co-bonded.

The second method (Ad) was adhesive bonding with the resin used as matrix in the composite skin sheets. The resin (Super Sap One, Entropy Resins) was applied to surfaces of the threaded skins and cores. The core and skins were bonded under vacuum (–0.6 bar).

The third method (Pr) was studied to apply to the PLA honeycomb cores and PLA-matrix based skins. This series (PF-PLA-Pr) was bonded by using a hot press (parameters: 185 °C, 2.0 bar). During hot pressing, only the outer surfaces of PLA-core reached melting temperature for bonding. It should noted that the PLA core did not heat up to 185 °C (melting) anywhere else than on the bond surfaces of the core splice.

Table 2: Test series in this study.

Series name	Matrix type (skin)	Fibre type (skin)	Core material	Bonding method
REF-G	UP	Glass	Cork	Filament-wound on core (co-bonded)
EF-EPS-Co	Epoxy	Flax	EPS	Co-bonded within skin lamination
EF-EPS-Ad	Epoxy	Flax	EPS	Cured skin sheets adhesively bonded
EF-CS-Ad	Epoxy	Flax	Cellulose foam	Cured skin sheets adhesively bonded
EF-PLA-Ad	Epoxy	Flax	PLA (3D-printed)	Cured skin sheets adhesively bonded
PF-PLA-Pr	PLA	Flax	PLA (3D-printed)	Hot press bonded after hot pressing of skins

UV-rain cabinet used for an aged condition of specimens

Environmental conditioning following the standard ASTM G155-13 was run except that the water spraying step was applied without radiation (ultraviolet (UV) radiation was applied in a separate step). The total test time was 500 hours meaning 250 two-hour cycles (a two hour cycle in Table 3). Specimen rotation in the conditioning chamber was performed to evenly apply conditioning to age the specimens from all sides. The cabinet was of model Q-sun Xe-3 (Q-lab). The specimens were aged without free-edge sealing to gain the most severe effect on the specimens used for testing (i.e., the aging effect here is test specimen geometry-dependent).

Table 3: UV radiation and rain spray used in this study for aging the specimens.

Step	Mode	Radiation intensity (W/m^2)	Black panel temperature (°C)	Air temperature (°C)	RH (%)	Time (min)
1	Radiation	0.35	63	48	30	102
2	Water spraying	0	38	21	90	18

Flatwise tensile testing

The Flatwise Tensile Strength (FTS) specimens were fabricated by following the standard ASTM C 297. From the sandwich panels, pieces were water jet-cut to a 20 mm × 20 mm size. Aluminium load blocks were glued (DP460, 3M) to the pieces for test jig connection. Specimens schematic is presented in Fig. 2 The bond surfaces were sanded and cleaned for the gluing. The glue was post-cured in the oven (50 °C, 24 hours). FTS specimens were tested by using a universal testing machine (5967, Instron) with computer control and data acquisition and with a 30 kN load cell. FTS testing was performed at a constant cross-head displacement rate of 1.0 mm/min. Displacement, load and time data were recorded at 25 Hz. Five specimens of every series reference (no aging) and UV-rain aged

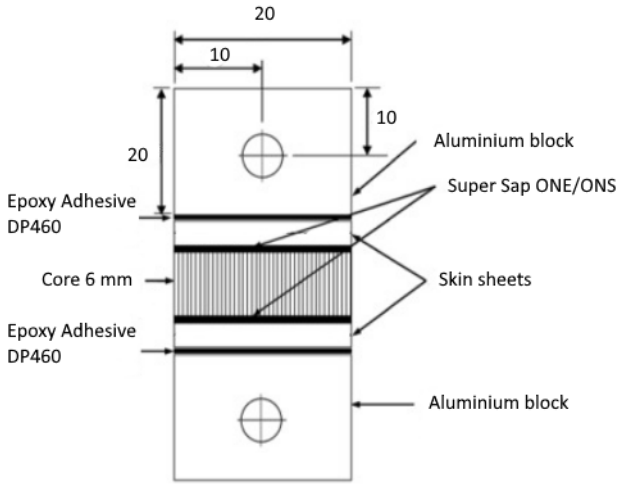

Figure 2: The schematic of the specimens for flat-wise tensile test resembling ASTM C297. All dimensions are in millimeters.

series per material system were tested. The (averaged) failure stress was calculated using force and cross-sectional area measured for each specimen. Failure strain was estimated based on the displacement data and was defined as the point of maximum stress (i.e., failure stress). Toughness was integrated as the area under the stress-strain curve; the change was calculated by comparing non-aged and aged specimens' results.

Notched single-lap shear testing

The Notched Single-lap Shear (NSS) specimens were manufactured by following the standard ASTM D 5868. Pieces of a size of 20 × 160 mm were water jet cut from the bonded panels. Crack slots for both sides (skins) were cut using a circular bench saw, adjusted to the thickness of the skin (Fig. 3). All the samples were stabilized in 50 ° C, 24 hours. The testing was performed using a test machine (5967, Instron), at a constant cross-head speed of 1 mm/s. From sandwich panels, pieces were water jet cut to a 20 mm × 160 mm size. Five specimens of every series reference (no aging) and UV-rain aged series per material system were prepared for testing. Ultimate (average) shear stress was calculated using force and cross-sectional area (between slots, nominal slot distance 25 mm) measured for each specimen. Shear strain (γ) was calculated based on:

$$\gamma = \arctan\left(\Delta d/t\right) , \tag{1}$$

where t is the core thickness and Δd is the axial displacement subjected to the test specimen by the test device. Here, it is presumed that the deformation in the stiff composite skin sheets is insignificant compared to core's deformation.

DIC system application for strain field imaging

2D-Digital Image Correlation (DIC) technique [13] was used to study the deformation of the core in flatwise tensile tests. The equipment consisted of a 5 Mpix CCD camera (Basler piA2400-17gm) and a bilateral telecentric lens. Before testing, a black-and-white random speckle pattern was applied on the specimens by spraying.

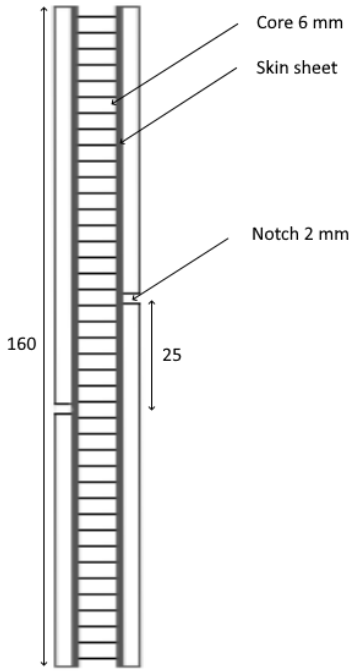

Figure 3: The schematic of the specimens for the NSS test resembling ASTM D 5868. All dimensions are in millimeters.

Recording rate of 5 frames per second was used. The captured images were processed with Davis 10.2.0 software (LaVision, Germany) into full-field strain distribution maps in the loading direction ('axial'). The strain fields at the onset of the specimen failure were used to investigate the localization of the damage in the specimen.

SEM imaging

Scanning electron microscopy (SEM) images were taken with JEOL (Variable pressure tungsten-filament SEM, model IT500). The samples were gold-sputtered except for EF-CS-Ad that was studied with the low vacuum operation mode without coating.

Results and Analysis

Out-of-plane tensile behavior

The cork-core of the reference series (REF-G) did not suffer significant aging in terms of FTS but mainly in terms of failure strain, i.e., cork was comparatively durable core material in the UV-rain environment. The series with EPS and adhesive bonding (EF-EPS-Ad) had similar behavior compared to the REF-G series but FTS was lower. The aging resulted in a similar decrease of FTS (–10 %) but greatly increased failure strain (+85 %). This is a good result for the EPS core, when considering the open edges of the specimens in this study. When the bonding technique was different (co-bonded), the results were very similar (decrease of FTS –7 % and increased failure strain +56 %). This suggests similar failure mode (cohesive failure) for both bonding techniques in these EPS series. One reference specimen of the series EF-EPS-Ad indicated brittle behavior due to core-skin sheet debonding indicated brittle behavior due to core-skin sheet debonding that is presumably flaw during manufacture of the specimens (Fig. 4 c). The increase in

the failure strain indicates increased plasticization of core material, in the case of cohesive failure, related to the aging by UV and rain.

When the core splice was changed into the cellulose foam, an interesting effect was observed. The naturally moisture-sensitive cellulosic core material restored the initial stiffness very well as indicated by the (decreased) series-average failure strain and a minor change in FTS (–4.4 %). This is partly due the fact that the foam is very compliant and the stress-strain curves tend to have plateau or repeated stress peaks. By looking at the curves overall, the non-aged and aged specimens have essentially similar behavior.

Table 4: Tensile out-of-plane test (FTS) results for sandwich specimens.

Series	Tensile failure stress (MPa)	Tensile strain at failure stress (m/m)	Toughness change due to aging (%)
REF-G	1.55 ± 0.25	0.07 ± 0.01	
REF-G (aged)	1.64 ± 0.31	0.08 ± 0.01	-11.5
EF-EPS-Ad	0.41 ± 0.04	0.05 ± 0.01	
EF-EPS-Ad (aged)	0.37 ± 0.12	0.09 ± 0.02	-9.5
EF-EPS-Co	0.48 ± 0.27	0.05 ± 0.02	
EF-EPS-Co (aged)	0.45 ± 0.11	0.08 ± 0.02	-2.2
EF-CS-Ad	0.036 ± 0.02	0.40 ± 0.19	
EF-CS-Ad (aged)	0.034 ± 0.02	0.20 ± 0.08	-48.2
EF-PLA-Ad	0.91 ± 0.53	0.03 ± 0.03	
EF-PLA-Ad (aged)	0.56 ± 0.23	0.08 ± 0.01	-5.9
PF-PLA-Pr	0.75 ± 0.34	0.05 ± 0.02	
PF-PLA-Pr (aged)	0.12 ± 0.08	0.04 ± 0.02	-85.3

The PLA honeycomb cores turned out to be very stiff and the failure mode of the sandwich specimens was mainly debonding at the interface of the skin sheet and core splice. The UV-rain aging resulted in a multiple debonding processes that included several onset points over a rather low stress level—FTS was in average 39 % lower due to aging. The change of the epoxy-based composite skins into PLA-matrix skins (and core bonding by hot press method) did not affect the non-aged specimens' behavior greatly (–17 % lower FTS). However, the interface between the PLA-flax reinforced composite skins and the PLA honeycomb splice, bonded by hot pressing, suffered significantly due to the UV-rain (decrease of FTS –84 %).

During the UV-rain aging, humidity significantly degraded the hot-pressed joint (Fig. 4 f) and caused failure at much lower forces. The failure surface is essentially the same, the polymer has simply weakened and got more brittle [17]. For thermosets as well as thermoplastics (e.g., PLA) hydrolysis is the expected main type of degradation. It is also presumed that the hot press method may have caused thermal residual stresses at the bond interface and the moisture during conditioning resulted in crack propagation due to residual stresses within the weakened polymer.

The toughness values indicated degradation for all the aged specimen series (–2 to –85 %). The most significant decrease in toughness was suffered by the EF-CS-Ad and PF-PLA-Pr series. Aged EF-EPS-Co, EF-EPS-Ad and EF-PLA-Ad series had less than 10 % effect on toughness due to degradation. These results essentially agree with the degradation of bio-materials, such as those based on cork and PLA [16] [17].

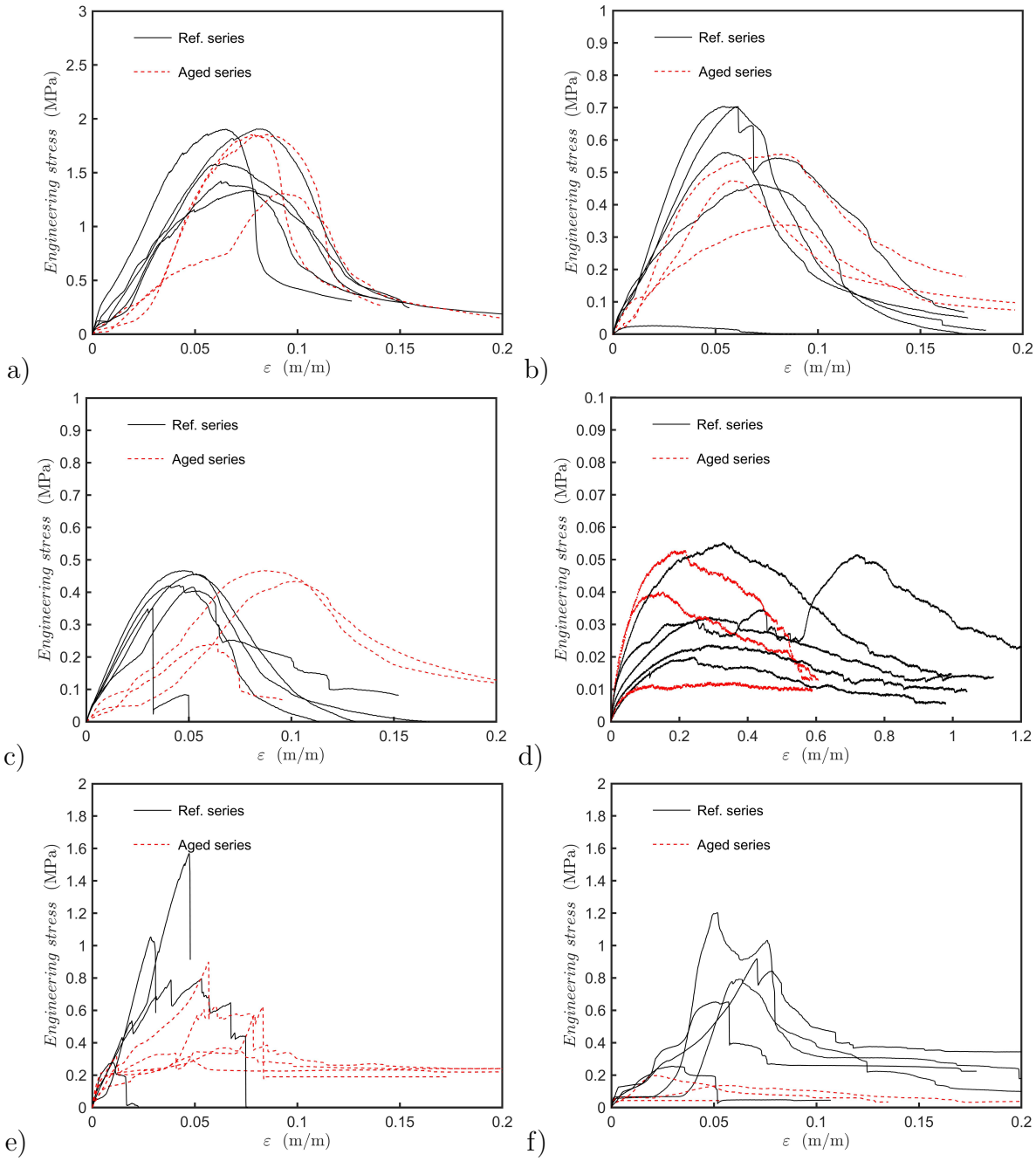

Figure 4: Tensile out-of-plane stress-strain behavior for different sandwich specimens: a) REF-G; b) EF-EPS-Ad; c) EF-EPS-Co; d) EF-CS-Ad; e) EF-PLA-Ad; f) PF-PLA-Pr. The code 'Ref-series' in the graphs refers to the non-aged specimens.

It should be noted that, for many of the FTS specimens, the core splice failed so that tiny strings or shreds were left unbroken and they could carry slight load after the specimen was practically failed. This resulted in essentially horizontal curves after failure in the data.

Shear behavior

The out-of-plane shear performance in general indicated similar tendency as the out-of-plane tensile behavior (in terms of FTS) for the sandwich structures. For the reference (REF-G) series, the shear behavior in terms of the shear failure stress degraded –15 % due to aging. For the specimens with EPS cores, the shear failure stress level was in general very low and the degradation due to UV-rain was ≈2 %. The bonding technique for the specimens with EPS cores had basically no effect when comparing intact and UV-rain conditioned specimens (change in shear failure stress –11 % and –23 %, for adhesive-bonded and co-bonded series, respectively).

In contrast, the series with the cellulosic foam splice suffered greatly due to the UV-rain conditioning (the decrease in failure shear stress –53 %). However, it is very interesting to note that the shear performance of CS core was better compared to the absolue values for the sandwich with EPS (both bonding techniques included). The shear failure stress values are higher for non-aged and aged CS test series than those of EPS series (100 % higher and 15 % higher for the non-aged and aged series, respectively). Behavior in cellulose foam is not isotropic because it has layered structure and chitosan addition might have increased durability against rain-UV. [14] [15]

For the PLA honeycomb cores, the shear behavior of the sandwich specimens had a similar tendency as it was for the FTS tests. The shear failure stress decreased –39 % and –62 %, for the epoxy-resin co-bonded and hot press-bonded specimens, respectively. Interestingly, the hot press-bonded sandwich specimens have relatively low experimental scatter (coefficient of variation 8 % and 6 %, for non-aged and aged series, respectively) in the failure stress values.

Table 5: Shear out-of-plane test (NSS) results for sandwich specimens.

Series	Shear failure stress (MPa)	Shear strain at failure stress (°)
REF-G	1.50 ± 0.05	13.7 ± 1.20
REF-G (aged)	1.28 ± 0.04	11.6 ± 0.96
EF-EPS-Ad	0.28 ± 0.01	11.6 ± 0.52
EF-EPS-Ad (aged)	0.25 ± 0.06	11.3 ± 4.25
EF-EPS-Co	0.29 ± 0.01	15.7 ± 1.80
EF-EPS-Co (aged)	0.22 ± 0.01	15.6 ± 4.48
EF-CS-Ad	0.57 ± 0.11	8.37 ± 1.97
EF-CS-Ad (aged)	0.27 ± 0.13	6.73 ± 0.71
EF-PLA-Ad	2.26 ± 0.47	14.6 ± 0.83
EF-PLA-Ad (aged)	1.37 ± 1.10	6.73 ± 2.99
PF-PLA-Pr	6.8 ± 0.51	9.3 ± 1.55
PF-PLA-Pr (aged)	2.3 ± 0.15	8.1 ± 1.30

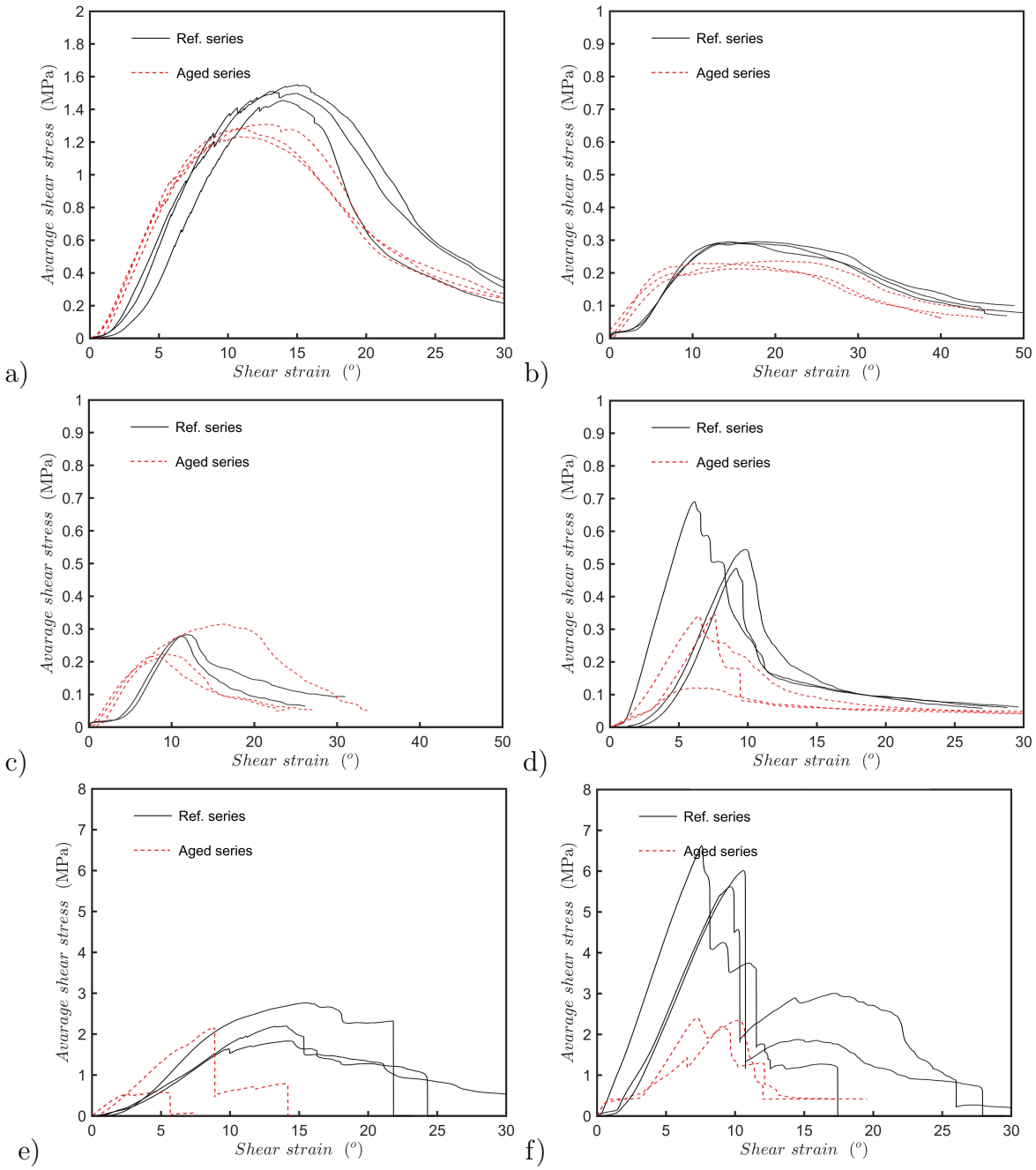

Figure 5: Shear out-of-plane test results for different sandwich specimens: a) REF-G; b) EF-EPS-Ad; c) EF-EPS-Co; d) EF-CS-Ad; e) EF-PLA-Ad; f) PF-PLA-Pr. The code 'Ref-series' in the graphs refers to the non-aged specimens.

Localization of damage in flatwise tensile tests

The qualitative DIC analysis for the axial strain fields at the onset of the failure in flatwise tensile test is presented in Figure 3. The figure depicts characteristic differences in the strain localization between the different core materials. Of the tested materials, the cork shows the most even strain distribution. The material deforms relatively uniformly and no single location can be named for the failure initiation spot.

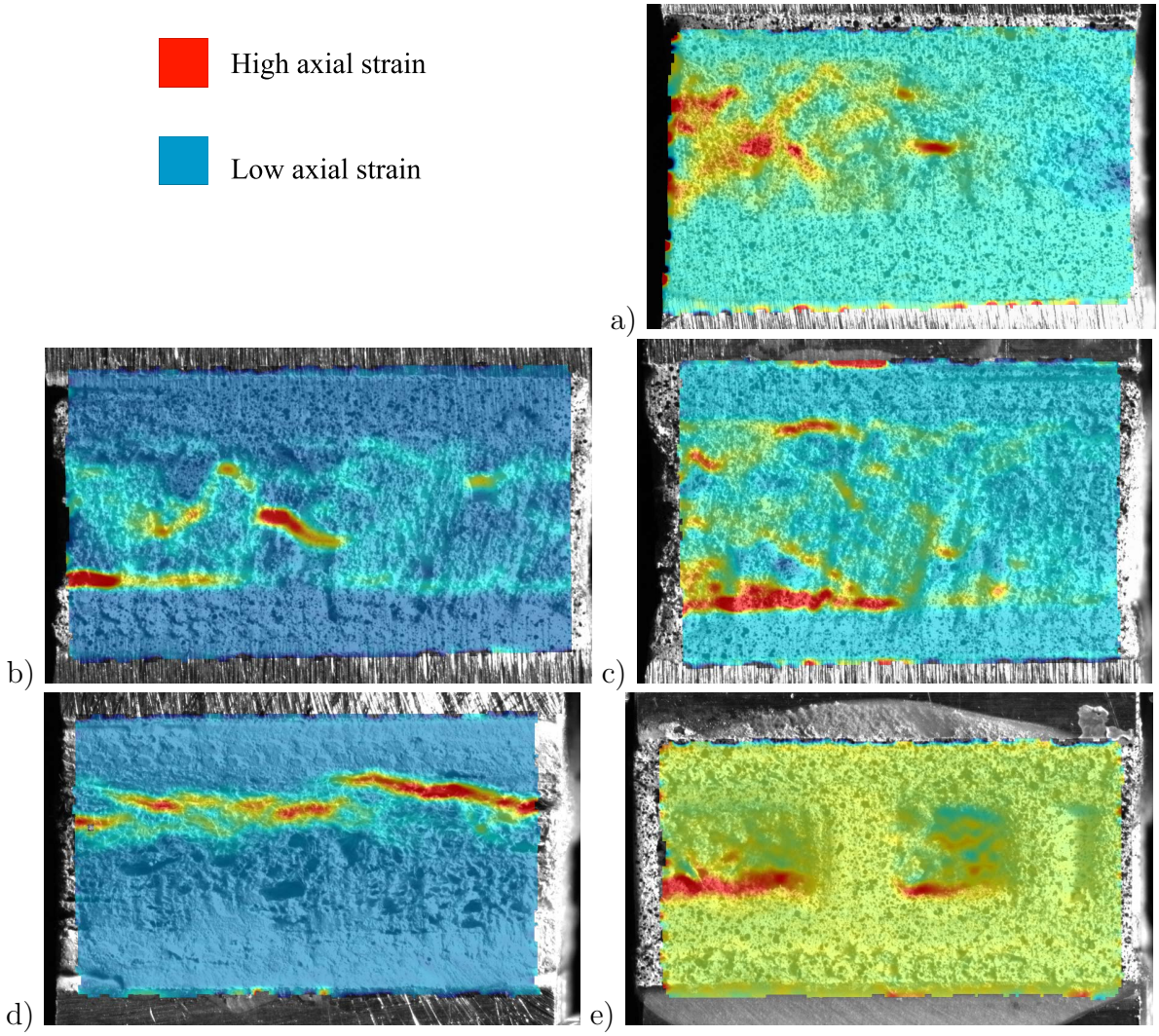

Figure 6: Qualitative axial strain (out-of-plane) distributions based on DIC imaging at the point of visual onset of damage: a) REF-G; b) EF-EPS-Ad; c) EF-EPS-Co; d) EF-CS-Ad; e) EF-PLA-Ad. The ultimate (high, low) strain levels as color codes are given above.

The specimens with EPS core show evident locations inside the core where the crack(s) begin to initiate. In addition to the high strain concentration spots in the core itself, it is also seen that the deformation localizes also at the skin-core interface. The deformation in the CS specimen localizes in a horizontal layer of the core, indicating heterogeneous mechanical properties of the material in the out-of-plane direction.

For the 3D-printed PLA honeycomb, the deformation is localized largely at the junction of the cell walls and the cell cap. The location of strain localization [11] can indicate the mode of failure in composite materials. The exact failure modes are discussed and analysed in the next section.

Micro-structure of core splices after testing

In Fig. 7 a, there is the cork granules' failed surface, which is full of air-filled voids between and inside the granules. Non-harmed granule surface is shown on the background. The image shows the morphology of natural cork's cellular structure and ruptured granule surfaces. Cork represents a cellular structure formed by thin-walled prismatic cells. A detailed analysis on the cellular structure reveals that the cellular voids represent most of the cork volume, which justifies its low density and most of its unique properties [12]. This structure is anticipated to bring in the even strain distribution observed in Fig. 6 for series REF-G. The cohesive rupture has been shown to be typical for cork-core sandwiches [17].

The EPS foam's fractured surface is seen in Fig. 7 b. The image is a holistic view of the fractured EPS structure in a sandwich system. In the middle of the image, epoxy resin (droplet) that has impregnated inside the foam structure can be seen. In addition to infused epoxy, there are air-filled voids of the ruptured EPS beads. This type of fracture surface represent the vicinity of the bond line, naturally.

The macro-structure of the failed CS surface can be seen in the SEM micrograph in Fig. 7 c. The cellulose fibres are irregular and the average distance and number of fibre-crossings (presumed contact points) between the fibres vary throughout the foam micro-structure. Overall, the cellulosic fibres are long—in the order of hundreds of microns [10]. Fibre sizes (diameter) are in the order of 20–40 µm. It should be noted that the integrity of foam-formed structure is largely based on inter-fibre bonds and the effect of additives.

In Fig. 7 d, a fractured PLA-honeycomb wall structure is seen for a specimen with failure in the core (cohesive). Failed strings of PLA—originating from the 3D-printing process—is seen on fracture surface (Fig. 7 d, 8). Mostly the surface is suggested to represent the interface between subsequent 3D-printing layers.

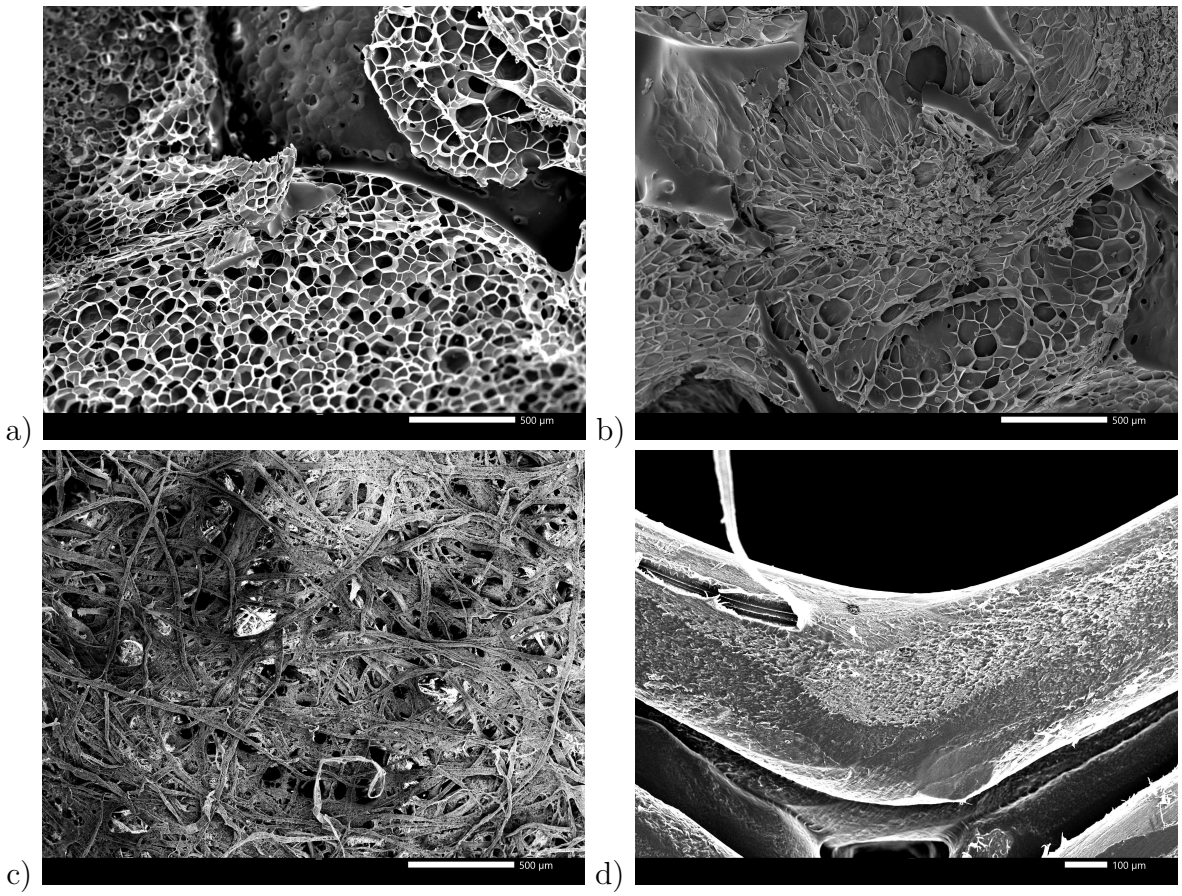

Figure 7: SEM analysis of the fracture surfaces after out-of-plane tensile testing of sandwich specimens: a) REF-G (scale bar 500 µm); b) EF-EPS-Ad (scale bar 500 µm); c) EF-CS-Ad (scale bar 500 µm); d) EF-PLA-Ad (scale bar 100 µm).

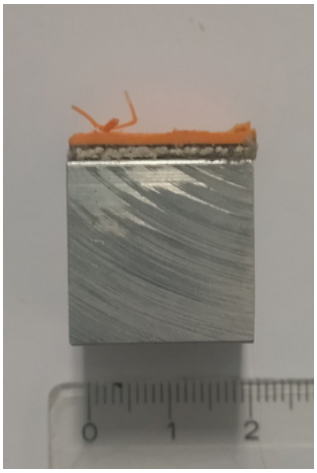

Figure 8: EF-PLA-Ad test series' typical core failure mode. The honeycomb cell structure failed at its root so that the 3D-printed flat base of the core splice is left attached to the metallic loading block. Dimensions in centimeters.

Conclusions

This study investigated the aging performance of sandwich structures with bio-based raw materials and 'green' design concepts. The reference structure was a glass reinforced polyester skin laminates and cork core. The candidate sandwich series were manufactured using partly bio-based epoxy and flax reinforcement for the skins as well as polylactic acid with flax reinforcement. The candidate core materials were expanded polystyrene, cellulose foam and 3D-printed honeycomb. The main goal was to study the effects of aging due to UV and rain conditioning.

The aging effect in the reference structures with cork core splices and glass fibre reinforced composite skins indicated a moderate aging effect overall (<16 %). The results for cellulose foam-integrated sandwich showed that these structures had comparable or even better mechanical performance under shearing load, including the degradation by UV-rain, than the structures with the EPS core. This finding was valid when the EPS core splice had approximately half of the density of cellulose foam. The 3D-printed PLA honeycomb sandwich structures had a high flatwise tensile strength (0.75–0.91 MPa) and shear failure stress (2.3–6.8 MPa) but also a big effect by the aging (even 84 % of decrease). The significant aging effect mainly affected the bond of the honeycomb PLA to the flax fibre-reinforced composite skins.

Further testing of bending and out-of-plane impact performance, as well as numerical simulation works, are necessary to continue the study of the promising bio-based core materials for composite sandwich structures.

Acknowledgments

This study was funded by the KAUTE foundation, and the ecosystem project SmartRail (Business Finland). This work made use of Tampere Microscopy Center facilities at Tampere University. The support from Mari Honkanen is also acknowledged.

References

[1] P.R. Oliveira, M. May, T.H. Panzera, S. Hiermaier. Bio-based/green sandwich structures: A review. Thin-Walled Structures, 177:109426, 2022. https://doi.org/10.1016/j.tws.2022.109426

[2] R.J. Tapper, M.L. Longana, A. Norton, K.D. Potter, I. Hamerton. An evaluation of life cycle assessment and its application to the closed-loop recycling of carbon fibre reinforced polymers. Composites Part B: Engineering, 184:107665, 2020. https://doi.org/10.1016/j.compositesb.2019.107665

[3] P. Glavic, R. Lukman. Review of sustainability terms and their definitions. Journal of Cleaner Production, 15(18):1875-1885, 2007. https://doi.org/10.1016/j.jclepro.2006.12.006

[4] T. Bayerl, M. Geith, A.A. Somashekar, D. Bhattacharyya. Influence of fibre architecture on the biodegradability of FLAX/PLA composites. International Biodeterioration & Biodegradation, 96:18-25, 2014. https://doi.org/10.1016/j.ibiod.2014.08.005

[5] S. Alsubari, M.Y.M. Zuhri, S.M. Sapuan, M.R. Ishak, R.A. Ilyas, M.R.M. Asyraf. Potential of natural fiber reinforced polymer composites in sandwich

structures: A review on its mechanical properties. Polymers, 13(3):423, 2021. https://doi.org/10.3390/polym13030423

[6] F. Bensadoun, I. Verpoest, J. Baets, J. Müssig, N. Graupner, P. Davies, M. Gomina, A. Kervoelen, C. Baley. Impregnated fibre bundle test for natural fibres used in composites. Journal of Reinforced Plastics and Composites, 36(13):942-957, 2017. https://doi.org/10.1177/0731684417695461

[7] Xiaoning Tang, Xiong Yan. A review on the damping properties of fiber reinforced polymer composites. Journal of Industrial Textiles, 49(6):693-721, 2018. https://doi.org/10.1177/1528083718795914

[8] I.M. Daniel, E.E. Gdoutos, K.A. Wang, J.L. Abot. Failure modes of composite sandwich beams. Journal of Damage Mechanics, 11(4):309-334, 2002. https://doi.org/10.1106/105678902027247

[9] M. Niu. Composite Airframe Structures: practical design information and data. 3^{rd} Edition. Hong Kong Conmilit Press Ltd, 2010. ISBN-13: 978-9627128069.

[10] T. Hjelt, J.A. Ketoja and H. Kiiskinen, A.I. Koponen, E. Pääkkönen. Foam forming of fiber products: a review. Journal of Dispersion Science and Technology, 3(5):12-15, 2021. https://doi.org/10.1080/01932691.2020.1869035

[11] N. Pournoori, G. Corrêa Soares, O. Orell, S. Palola, M. Hokka, M. Kanerva. Adiabatic heating and damage onset in a pultruded glass fiber reinforced composite under compressive loading at different strain rate. International Journal of Impact Engineering, 147:103728, 2021. https://doi.org/10.1016/j.ijimpeng.2020.103728

[12] H. Pereira. The Rationale behind Cork Properties: A Review of Structure and Chemistry. BioResources, 10(7):2-5, 2015. https://doi.org/10.1177/1528083718795914

[13] Jones, E.M.C, Iadicola, M. A. A Good Practices Guide for Digital Image Correlation. International Digital Image Correlation Society, 94, 2018.

[14] D. Alonso, M. Gimeno, R. Olayo, H. Vâzquez-Torres, J. D. Sepûlveda-Sânchez, K. Shirai. Cross-linking chitosan into UV-irradiated cellulose fibers for the preparation of antimicrobial-finished textiles. Carbohydrate Polymers, 77(3):536-543, 2009. https://doi.org/10.1016/j.carbpol.2009.01.027

[15] A. Ottenhall, T. Seppänen, M. Ek. Water-stable cellulose fiber foam with antimicrobial properties for bio based low-density materials. Cellulose, 25, 2599-2613, 2018. https://doi.org/10.1007/s10570-018-1738-y

[16] S. Prabhakaran, V. Krishnaraj, H. Golla, M. Senthilkumar. Biodegradation behaviour of green composite sandwich made of flax and agglomerated cork. Polymers and Polymer Composites, 30, 2022. https://doi.org/10.1177/09673911221103602

[17] MC. Mistretta ,FP. La Mantia,V. Titone, L. Botta, M. Pedeferri, M. Morreale. Effect of ultraviolet and moisture action on biodegradable polymers and their blend. Journal of Applied Biomaterials and Functional Materials, 18, 2020. https://doi.org/10.1177/2280800020926653

Pauli Hakala, Olli Orell, Essi Sarlin, Mikko Kanerva
Tampere University
Materials Science and Environmental Engineering unit
Korkeakoulunkatu 10, Tampere, Finland
pauli.hakala@tuni.fi, olli.orell@tuni.fi, essi.sarlin@tuni.fi, mari.honkanen@tuni.fi, mikko.kanerva@tuni.fi

Elina Pääkkönen
VTT Technical Research Centre of Finland Ltd
Solutions for Natural Resources and Environment
Koivurannantie 1, FI-40400 Jyväskylä, Finland
Elina.Paakkonen@vtt.fi

Lauri Jutila
CSI Composites Oy
Virtaintie 15, Mänttä-Vippula, Finland
lauri.jutila@csi-composites.fi